Opposing effects of Elk-1 multisite phosphorylation shape its response to ERK activation

Anastasia Mylona[1*], Francois-Xavier Theillet[2*], Charles Foster[1], Tammy M. Cheng[3], Francesc Miralles[4], Paul A. Bates[3], Philipp Selenko[2], Richard Treisman[1]†

[1]Signalling and Transcription Laboratory, The Francis Crick Institute, Lincoln's Inn Fields Laboratory, 44 Lincoln's Inn Fields, London WC2A 3LY, UK.

[2]In-Cell NMR Laboratory, Department of NMR-supported Structural Biology, Leibniz Institute of Molecular Pharmacology (FMP Berlin), Berlin, Germany.

[3]Biomolecular Modelling Laboratory, The Francis Crick Institute, Lincoln's Inn Fields Laboratory, 44 Lincoln's Inn Fields, London WC2A 3LY, UK.

[4]Molecular & Clinical Sciences Research Institute, St. George's, University of London, London SW17 0RE, UK.

*current addresses: AM, Faculty of Life Sciences & Medicine, Guy's Campus, Kings' College London, London SE1 1UL, UK; F-XT, Institute of Integrative Biology of the Cell (I2BC), CNRS/CEA/Paris-Saclay University, 91191 Gif-sur-Yvette, France.

† Corresponding authors E-mail: Richard.Treisman@crick.ac.uk

Abstract (119 words)

Multisite phosphorylation regulates many transcription factors, including the Serum Response Factor partner Elk-1. Phosphorylation of the transcriptional activation domain (TAD) of Elk-1 by the protein kinase ERK at multiple sites potentiates recruitment of the Mediator transcriptional coactivator complex and transcriptional activation, but the roles of individual phosphorylation events remained unclear. Using time-resolved nuclear magnetic resonance spectroscopy, we found that ERK2 phosphorylation proceeds at markedly different rates at eight TAD sites *in vitro*, which we classified as fast, intermediate and slow. Mutagenesis experiments showed that phosphorylation of fast and intermediate sites promoted Mediator interaction and transcriptional activation, whereas modification of slow sites counteracted both functions, thereby limiting Elk-1 output. Progressive Elk-1 phosphorylation thus ensures a self-limiting response to ERK activation, which occurs independently of antagonizing phosphatase activity.

RESULTS AND DISCUSSION

Multisite protein phosphorylation increases the complexity of functional signaling outputs that can be generated from single protein kinase inputs. It can set thresholds for activity, or transform graded signals into switch-like responses (*1-4*). Many transcription factors and their interacting regulatory proteins are subject to multisite phosphorylation, which allows distinct aspects of protein function, including protein turnover, nuclear import and export, and specific protein interactions, to be controlled independently (*5*). However, in general, the dynamics and functional roles of individual phosphorylation events are incompletely understood.

The ternary complex factor (TCF) subfamily of Ets-domain transcription factors, consisting of Elk-1, SAP-1, and Net, provides an example of multisite phosphorylation in transcriptional activation. TCFs, together with their partner protein SRF, function in many biological processes by coupling SRF target genes to mitogen-activated protein kinase (MAP kinase) signaling (*5*). Mitogenic and stress stimuli induce phosphorylation of TCF C-terminal transcriptional activation domains (TADs) at multiple S/T-P (Ser- or Thr-Pro) phosphorylation sequences, of which eight are conserved across the family (Fig. 1A; fig. S1) (*6-11*). Two MAP kinase-docking sites, the D-box and the Phe-Gln-Phe-Pro (FQFP) motif, control phosphorylation of these sites (*12-15*). Multisite phosphorylation triggers transcriptional activation by TCFs, facilitating their interaction with the Mediator transcriptional co-activator complex (*16-19*) but the kinetics with which the different sites are phosphorylated, and whether they serve distinct functions, remain unclear.

To obtain atomic-resolution insights into phosphorylation of the Elk-1 TAD, we used nuclear magnetic resonance (NMR) spectroscopy (*20*) to monitor its modification by recombinant ERK2 *in vitro* (Fig. 1B; fig. S2A). Time-resolved NMR experiments revealed that each phosphorylation proceeded efficiently, but at markedly different rates. Phosphorylation of Thr^{369} and Ser^{384}, which flank the central Phe–Trp (FW) motif implicated in Mediator interaction (*18*), occurred faster than modification of Thr^{364}, Thr^{354} and Ser^{390}, whereas residues Thr^{418}, Ser^{423} and Thr^{337} were modified more slowly (Fig. 1C), which we confirmed by immunoblotting (Fig. 1D). Chemical shift analysis (Cα, Cβ) showed no stable secondary structure elements in unmodified or phosphorylated Elk-1 TAD (fig. S2B).

As a first step towards understanding the basis for the phosphorylation sites' differential kinetic behavior, we devised a reaction model based on Michaelis-Menten enzyme kinetics. To simplify the mathematical treatment, we grouped Elk-1 sites into three classes: fast (Thr^{369} and Ser^{384}), intermediate (Thr^{354}, Thr^{364}, and Ser^{390}) and slow (Thr^{337}, Thr^{418}, and Ser^{423}). We assumed that ERK2 phosphorylation is distributive, that enzymatic rate constants (k_{cat}) are similar for all sites, and that the different sites have relative affinities for ERK2 modeled by increasing Michaelis-Menten constants ($K_M^{Fast} < K_M^{Int} < K_M^{Slow}$)(Fig. 2A, fig. S3A, *20*). This model, which recapitulated the measured kinetics of *in vitro* Elk-1 phosphorylation well (Fig. 2B) predicted that removal of fast or intermediate sites should increase the phosphorylation rates of other sites. To test this idea, we analyzed the phosphorylation kinetics of Elk-1 TAD mutants in which we substituted all fast or intermediate phosphoacceptor residues with alanines (Elk-1F:

Thr^{369}→Ala, Ser^{384}→Ala; Elk-1I: Thr^{354}→Ala, Thr^{364}→Ala, and Ser^{390}→Ala)(Fig. 2A). In the fast site mutant Elk-1F, phosphorylation rates of intermediate and slow sites increased, whereas those of the fast and slow sites increased in the intermediate-site mutant Elk-1I; in both cases the altered kinetics fit well with those predicted by the model (Fig 2B, fig. S3B). Thus, even the fast sites are not phosphorylated at the maximum possible rate in the wildtype protein. Moreover, phosphorylation of an Elk-1 TAD mutant in which Thr^{369} and Ser^{384} were replaced with aspartates was similar to Elk-1F, excluding the possibility that fast-site phosphorylation primes later modification events (fig. S3B).

To gain more insight into the factors affecting individual sites' phosphorylation kinetics, we assessed the role played by primary sequence. To do this, we exchanged the sequences surrounding the fast Thr^{369} and slow Ser^{423} sites. This also effectively exchanged their reactivities, which suggests that these sites' phosphorylation rates reflect their position relative to ERK docking sequences, rather than intrinsic differences in reactivity (Fig. 2C). We therefore examined the contributions of the D-box and FQFP ERK docking motifs to each site's phosphorylation kinetics. Deletion of the D-box decreased the rates of Thr^{337}, Thr^{354}, Thr^{364} and Thr^{369} phosphorylation, but increased the rates of Ser^{390}, Thr^{418}, and Ser^{423} modification (Fig. 2D). In contrast, deletion of the FQFP motif decreased the rate of Ser^{384} phosphorylation, but enhanced modification of intermediate sites, including adjacent Ser^{390}, with no effect on the C-terminal sites (Fig. 2D). Thus, the ERK docking motifs differentially affect each phosphorylation site's competitive behavior. Previous studies showed that Elk-1 TAD phosphorylation by JNK

and p38 MAP kinase differs from phosphorylation by ERK (*10, 21-24*), and that this reflects differences in their docking interactions (*12, 14, 15, 25*). Indeed, these kinases exhibited site preferences and phosphorylation rates that were distinct from that of ERK2 (fig. S3C). Taken together, our results show that the different rates of Elk-1 TAD phosphorylation by ERK2 follow a competition mechanism that is governed by the position of individual Elk-1 substrate sites relative to ERK2 docking interactions.

To test whether the different kinetic classes of Elk-1 TAD phosphorylation sites are functionally equivalent, we expressed mouse Elk-1 mutants in fibroblasts derived from TCF-deficient ($Elk1^{-/-}$;$Elk3^{\delta/\delta}$;$Elk4^{-/-}$) triple-knockout mouse embryos (TKO MEFs; fig. S4, A-C). In these cells, immediate-early (IE) gene expression is defective, but expression of wild-type mouse Elk-1 restored the IE transcriptional activation seen in wild-type MEFs after activation of ERK by treatment with TPA (12-O-tetradecanoylphorbol-13-acetate) (fig. S4D). As expected, alanine substitutions of fast and/or intermediate sites, or of the FW motif, greatly diminished or abolished the ability of Elk-1 to activate TCF-SRF target gene transcription after TPA stimulation (Fig. 3A; fig. S4D). Surprisingly, however, mutation of the slow sites substantially enhanced Elk-1-mediated activation of TCF-SRF target genes (Fig. 3A). Alanine substitutions at individual slow sites also increased Elk-1 activity, with Thr^{418} exhibiting the greatest effect (Fig. 3B, fig. S4, E-G). TCF-SRF signaling is important for cellular proliferation (*26, 27*), and TKO MEFs proliferate more slowly than wildtype MEFs. The reconstituted TKO MEFs exhibited enhanced proliferation rates, which correlated with the ability of each mutant to promote transcriptional activation (Fig. 3C).

Phosphorylation of Elk-1 promotes transcriptional activation by facilitating its MED23-dependent interaction with the Mediator complex (*16-18*). We therefore investigated whether the different transcriptional activities of the Elk-1 mutants reflected alterations in Mediator binding. We prepared extracts of TKO cells expressing wildtype or mutant Elk-1 proteins and assessed Elk-1 assocation with Mediator by co-immunoprecipitation of the MED23, MED24 and MED16 subunits. Consistent with the transcription experiments, Elk-1–Mediator interaction was induced by TPA stimulation and dependent on the FW motif; it was abolished by alanine substitutions of fast and intermediate sites, and was increased in the slow-site Elk-1 mutant (Fig. 3D). We obtained similar results when we used glutathione *S*-transferase (GST)-Elk-1 TAD proteins to recover Mediator proteins from unstimulated NIH3T3 cell extracts (Fig. 3E). In this assay, ERK2 phosphorylation time-course experiments showed that Mediator recovery by the wildtype Elk-1 TAD was most efficient prior to modifications of the slow sites (fig. S5, A and B). Taken together, these data show that according to the sites involved, ERK2 phosphorylation promotes or inhibits transcriptional activation by Elk-1, which reflects alterations in Elk-1–Mediator interactions.

Next, we investigated Elk-1 TAD phosphorylation kinetics *in vivo*. Previous studies were unable to distinguish the progressive phosphorylation of fast and slow Elk-1 sites (*6*). However, by incubating cells at 25° C to slow down reactions, we confirmed that phosphorylation rates can be ranked in the order Ser^{384}>Thr^{364}>Thr^{418}, and that different site classes exhibited a similar competitive behavior, as seen *in vitro* (fig. S6A). Reasoning that phosphorylation of the Elk-1 TAD might be sensitive to kinetic effects at limiting signal strengths, we titrated ERK activity using increasing amounts of TPA. This

both increased the maximal extent of ERK activation and advanced the time at which it occurred (fig. S6B). At low TPA concentrations, Elk-1 fast-site (Thr^{384}) and slow-site (Thr^{418})-site modifications accumulated slowly over 1 hour, whereas at a saturating TPA dose they were maximal by 10 minutes. Both phosphorylations declined at late times, presumably owing to the action of Elk-1 phosphatases (Fig. 4A)(*6, 28*).

Having established that Elk-1 phosphorylation kinetics are tuned by signal strength, we investigated their relationship to transcriptional activation. We compared the ability of wildtype Elk-1 and the slow-site mutant Elk-1S to activate transcription in response to signals of differing strengths. At saturating TPA concentrations, both proteins activated *Egr1* transcription with similar transient kinetics, although Elk-1S was much more active, reflecting the loss of the inhibitory sites (Fig. 4, B and C). At limiting TPA doses, however, their behaviors were markedly different. Whereas the activity of wildtype Elk-1 was almost maximal by 15 minutes, that of Elk-1S increased substantially beyond this time (Fig. 4B), resulting in prolonged *Egr1* mRNA accumulation (Fig. 4C). Thus, progressive phosphorylation of the Elk-1 TAD by a single kinase, ERK, attenuates the transcriptional response of Elk-1, shaping it according to the strength and kinetics of ERK activation.

Our results show that phosphorylation of the Elk-1 TAD by a single kinase, ERK, can either promote or inhibit Mediator interaction, depending on the sites involved, thereby modulating transcriptional activation. Given that the TAD sequences are conserved in the other TCFs, our findings may also apply to them. The more rapidly phosphorylated sites are located in the substantially conserved central core of the TAD, and are essential for transcriptional activation, lying close to the FW hydrophobic motif

required for Elk-1–Mediator interaction (*10, 18*). Multisite phosphorylation of these residues might stabilize this interaction, and perhaps also set a signaling threshold for it, similar to the way that multisite phosphorylation sets a threshold for the Sic1–Cdc4 interaction (*29*). In contrast, slowly phosphorylated sites located N- and C-terminal of the conserved TAD core act negatively. Their phosphorylation inhibits Mediator recruitment and limits transcriptional activation (Fig 4D), and may also facilitate recruitment of negative regulators of Elk-1 activity. Together these properties ensure that ERK phosphorylation of the Elk-1 TAD is self-limiting, whereby phosphorylation of slow sites attenuates TCF-SRF target gene expression under conditions of strong or sustained ERK signaling (Fig. 4D). Our results challenge the common assumption that multisite modification events act unidirectionally and can only be reversed or limited by antagonistic enzymes. Given the prevalence of such events in different biological processes, we expect that similar mechanisms may govern other regulatory interactions.

REFERENCES

1. J. Gunawardena, Multisite protein phosphorylation makes a good threshold but can be a poor switch. *Proceedings of the National Academy of Sciences of the United States of America* **102**, 14617-14622 (2005); published online EpubOct 11 (10.1073/pnas.0507322102).

2. J. Gunawardena, Distributivity and processivity in multisite phosphorylation can be distinguished through steady-state invariants. *Biophysical journal* **93**, 3828-3834 (2007); published online EpubDec 1 (10.1529/biophysj.107.110866).

3. C. Salazar, T. Hofer, Multisite protein phosphorylation--from molecular mechanisms to kinetic models. *The FEBS journal* **276**, 3177-3198 (2009); published online EpubJun (10.1111/j.1742-4658.2009.07027.x).

4. X. Liu, L. Bardwell, Q. Nie, A combination of multisite phosphorylation and substrate sequestration produces switchlike responses. *Biophysical journal* **98**, 1396-1407 (2010); published online EpubApr 21 (10.1016/j.bpj.2009.12.4307).

5. M. Karin, T. Hunter, Transcriptional control by protein phosphorylation: signal transmission from the cell surface to the nucleus. *Current biology : CB* **5**, 747-757 (1995).

6. F. H. Cruzalegui, E. Cano, R. Treisman, ERK activation induces phosphorylation of Elk-1 at multiple S/T-P motifs to high stoichiometry. *Oncogene* **18**, 7948-7957 (1999); published online EpubDec 23 (10.1038/sj.onc.1203362).

7. R. Janknecht, W. H. Ernst, V. Pingoud, A. Nordheim, Activation of ternary complex factor Elk-1 by MAP kinases. *The EMBO journal* **12**, 5097-5104 (1993).

8. R. Marais, J. Wynne, R. Treisman, The SRF accessory protein Elk-1 contains a growth factor-regulated transcriptional activation domain. *Cell* **73**, 381-393 (1993).

9. R. Janknecht, W. H. Ernst, A. Nordheim, SAP1a is a nuclear target of signaling cascades involving ERKs. *Oncogene* **10**, 1209-1216 (1995).

10. M. A. Price, A. E. Rogers, R. Treisman, Comparative analysis of the ternary complex factors Elk-1, SAP-1a and SAP-2 (ERP/NET). *The EMBO journal* **14**, 2589-2601 (1995).

11. H. Gille, M. Kortenjann, O. Thomae, C. Moomaw, C. Slaughter, M. H. Cobb, P. E. Shaw, ERK phosphorylation potentiates Elk-1-mediated ternary complex formation and transactivation. *The EMBO journal* **14**, 951-962 (1995).

12. D. A. Fantz, D. Jacobs, D. Glossip, K. Kornfeld, Docking sites on substrate proteins direct extracellular signal-regulated kinase to phosphorylate specific residues. *The Journal of biological chemistry* **276**, 27256-27265 (2001); published online EpubJul 20 (10.1074/jbc.M102512200).

13. S. H. Yang, P. R. Yates, A. J. Whitmarsh, R. J. Davis, A. D. Sharrocks, The Elk-1 ETS-domain transcription factor contains a mitogen-activated protein kinase targeting motif. *Molecular and cellular biology* **18**, 710-720 (1998).

14. S. H. Yang, A. J. Whitmarsh, R. J. Davis, A. D. Sharrocks, Differential targeting of MAP kinases to the ETS-domain transcription factor Elk-1. *The EMBO journal* **17**, 1740-1749 (1998); published online EpubMar 16 (10.1093/emboj/17.6.1740).

15. D. Jacobs, D. Glossip, H. Xing, A. J. Muslin, K. Kornfeld, Multiple docking sites on substrate proteins form a modular system that mediates recognition by ERK MAP kinase. *Genes & development* **13**, 163-175 (1999).

16. J. L. Stevens, G. T. Cantin, G. Wang, A. Shevchenko, A. Shevchenko, A. J. Berk, Transcription control by E1A and MAP kinase pathway via Sur2 mediator subunit. *Science* **296**, 755-758 (2002); published online EpubApr 26 (10.1126/science.1068943).

17. G. Wang, M. A. Balamotis, J. L. Stevens, Y. Yamaguchi, H. Handa, A. J. Berk, Mediator requirement for both recruitment and postrecruitment steps in transcription initiation. *Molecular cell* **17**, 683-694 (2005); published online EpubMar 4 (10.1016/j.molcel.2005.02.010).

18. M. A. Balamotis, M. A. Pennella, J. L. Stevens, B. Wasylyk, A. S. Belmont, A. J. Berk, Complexity in transcription control at the activation domain-mediator interface. *Science signaling* **2**, ra20 (2009)10.1126/scisignal.1164302).

19. W. Wang, L. Huang, Y. Huang, J. W. Yin, A. J. Berk, J. M. Friedman, G. Wang, Mediator MED23 links insulin signaling to the adipogenesis transcription cascade. *Developmental cell* **16**, 764-771 (2009); published online EpubMay (10.1016/j.devcel.2009.04.006).

20. F. X. Theillet, H. M. Rose, S. Liokatis, A. Binolfi, R. Thongwichian, M. Stuiver, P. Selenko, Site-specific NMR mapping and time-resolved monitoring of serine and threonine phosphorylation in reconstituted kinase reactions and mammalian cell extracts. *Nature protocols* **8**, 1416-1432 (2013)10.1038/nprot.2013.083).

21. M. Cavigelli, F. Dolfi, F. X. Claret, M. Karin, Induction of c-fos expression through JNK-mediated TCF/Elk-1 phosphorylation. *The EMBO journal* **14**, 5957-5964 (1995).

22. H. Gille, T. Strahl, P. E. Shaw, Activation of ternary complex factor Elk-1 by stress-activated protein kinases. *Current biology : CB* **5**, 1191-1200 (1995).

23. A. J. Whitmarsh, P. Shore, A. D. Sharrocks, R. J. Davis, Integration of MAP kinase signal transduction pathways at the serum response element. *Science* **269**, 403-407 (1995).

24. M. A. Price, F. H. Cruzalegui, R. Treisman, The p38 and ERK MAP kinase pathways cooperate to activate Ternary Complex Factors and c-fos transcription in response to UV light. *The EMBO journal* **15**, 6552-6563 (1996).

25. D. L. Sheridan, Y. Kong, S. A. Parker, K. N. Dalby, B. E. Turk, Substrate discrimination among mitogen-activated protein kinases through distinct docking sequence motifs. *The Journal of biological chemistry* **283**, 19511-19520 (2008); published online EpubJul 11 (10.1074/jbc.M801074200).

26. E. R. Vickers, A. Kasza, I. A. Kurnaz, A. Seifert, L. A. Zeef, A. O'Donnell, A. Hayes, A. D. Sharrocks, Ternary complex factor-serum response factor complex-regulated gene activity is required for cellular proliferation and inhibition of

apoptotic cell death. *Molecular and cellular biology* **24**, 10340-10351 (2004); published online EpubDec (10.1128/MCB.24.23.10340-10351.2004).

27. M. A. Wozniak, C. Q. Cheng, C. J. Shen, L. Gao, A. O. Olarerin-George, K. J. Won, J. B. Hogenesch, C. S. Chen, Adhesion regulates MAP kinase/ternary complex factor exchange to control a proliferative transcriptional switch. *Current biology : CB* **22**, 2017-2026 (2012); published online EpubNov 6 (10.1016/j.cub.2012.08.050).

28. T. Sugimoto, S. Stewart, K. L. Guan, The calcium/calmodulin-dependent protein phosphatase calcineurin is the major Elk-1 phosphatase. *The Journal of biological chemistry* **272**, 29415-29418 (1997).

29. P. Nash, X. Tang, S. Orlicky, Q. Chen, F. B. Gertler, M. D. Mendenhall, F. Sicheri, T. Pawson, M. Tyers, Multisite phosphorylation of a CDK inhibitor sets a threshold for the onset of DNA replication. *Nature* **414**, 514-521 (2001); published online EpubNov 29 (10.1038/35107009).

30. M. K. Vartiainen, S. Guettler, B. Larijani, R. Treisman, Nuclear actin regulates dynamic subcellular localization and activity of the SRF cofactor MAL. *Science* **316**, 1749-1752 (2007); published online EpubJun 22 (10.1126/science.1141084).

31. A. Ayed, F. A. Mulder, G. S. Yi, Y. Lu, L. E. Kay, C. H. Arrowsmith, Latent and active p53 are identical in conformation. *Nature structural biology* **8**, 756-760 (2001); published online EpubSep (10.1038/nsb0901-756).

32. K. Tamiola, B. Acar, F. A. Mulder, Sequence-specific random coil chemical shifts of intrinsically disordered proteins. *Journal of the American Chemical Society* **132**, 18000-18003 (2010); published online EpubDec 29 (10.1021/ja105656t).

33. K. Tamiola, F. A. Mulder, Using NMR chemical shifts to calculate the propensity for structural order and disorder in proteins. *Biochemical Society transactions* **40**, 1014-1020 (2012); published online EpubOct (10.1042/BST20120171).

34. S. Schwarzinger, G. J. Kroon, T. R. Foss, J. Chung, P. E. Wright, H. J. Dyson, Sequence-dependent correction of random coil NMR chemical shifts. *Journal of the American Chemical Society* **123**, 2970-2978 (2001).

35. E. A. Bienkiewicz, K. J. Lumb, Random-coil chemical shifts of phosphorylated amino acids. *Journal of biomolecular NMR* **15**, 203-206 (1999).

36. G. Platzer, M. Okon, L. P. McIntosh, pH-dependent random coil (1)H, (13)C, and (15)N chemical shifts of the ionizable amino acids: a guide for protein pK a measurements. *Journal of biomolecular NMR* **60**, 109-129 (2014); published online EpubNov (10.1007/s10858-014-9862-y).

37. P. Patwardhan, W. T. Miller, Processive phosphorylation: mechanism and biological importance. *Cellular signalling* **19**, 2218-2226 (2007); published online EpubNov (10.1016/j.cellsig.2007.06.006).

38. M. Putz, A. Lacrama, V. Ostafe, Full Analytic Progress Curves of Enzymic Reactions in Vitro. *Int. J. Mol. Sci.* **7**, 469-484 (2006). doi:10.3390/i7110469

39. F. X. Theillet, H. M. Rose, S. Liokatis, A. Binolfi, R. Thongwichian, M. Stuiver, P. Selenko, Corrigendum: Site-specific NMR mapping and time-resolved monitoring of serine and threonine phosphorylation in reconstituted kinase reactions and mammalian cell extracts. *Nature protocols* **11**, 192 (2016); published online EpubJan (10.1038/nprot0116-192a).

40. P. Costello, R. Nicolas, J. Willoughby, B. Wasylyk, A. Nordheim, R. Treisman, Ternary complex factors SAP-1 and Elk-1, but not net, are functionally equivalent in thymocyte development. *Journal of immunology* **185**, 1082-1092 (2010); published online EpubJul 15 (10.4049/jimmunol.1000472).

41. A. Mylona, R. Nicolas, D. Maurice, M. Sargent, D. Tuil, D. Daegelen, R. Treisman, P. Costello, The essential function for serum response factor in T-cell development reflects its specific coupling to extracellular signal-regulated kinase signaling. *Molecular and cellular biology* **31**, 267-276 (2011); published online EpubJan (10.1128/MCB.01058-10).

ACKNOWLEDGEMENTS

Work in the Treisman group was supported by the Francis Crick Institute, which receives its core funding from Cancer Research UK (FC001-190), the UK Medical Research Council (FC001-190) and the Wellcome Trust (FC001-190); and by European Research Council (ERC) advanced grant 268690 ACTINonSRF. Work in the Selenko group is funded by the ERC consolidator grant #647474 NeuroInCellNMR. F.-X.T. is supported by Agence Nationale pour la Recherche grant ANR14-ACHN-0015-01. The authors have no conflicts of interest. AM conceived the project; A.M., C.F., and F.M. designed and performed molecular and cell biology experiments; F.X.-T., T.C. and P.B. developed the competitive inhibition model; F.-X.T. and P.S. designed, executed and interpreted the NMR experiments, and A.M., P.S. and R.T. designed and interpreted experiments and wrote the paper. We thank F. Gualdrini, C. Esnault and P. Costello for characterising gene regulation in reconstituted TKO MEFs, sharing their unpublished data, and generating reconstituted TKO MEF cells; the Crick Genomics and Flow Cytometry technology platforms for technical support; and A. Behrens, V. Calleja, A. Chakraborty, M. Diefenbacher, C. Duellberg, R. Nicolas, P. Riou, M. Skehel, and our group members for advice and discussions.

SUPPPLEMENTARY MATERIALS

Materials and Methods

Figs. S1 to S6

FIGURE LEGENDS

Figure 1. Multisite phosphorylation of Elk-1 TAD. (**A**) Linear outline of Elk-1 fast (red), intermediate (blue), and slow (yellow) S/T-P phosphorylation sites. Kinase docking motifs are shown in green; the FW residues (purple) are essential for Mediator association. (**B**) NMR analysis of Elk-1 TAD (amino acids 309 to 429) phosphorylation with recombinant ERK2. Left: 2D ^{1}H-^{15}N NMR spectrum of unphosphorylated Elk-1 (black), with phosphorylation-site signals color-coded as in (A). Right: overlay of 2D NMR spectra of phosphorylated [grey & color-coded as in (A)] and unmodified Elk-1 (black). (**C**) Time-resolved modification curves of individual Elk-1 sites upon phosphorylation with ERK2; error bars denote differences between replicate experiments on two independent samples. (**D**) Time-course Western blot of GST-Elk-1 TAD phosphorylation and phosphorlyation-site-specific antibody detection.

Figure 2. Phosphorylation kinetics of Elk-1 TAD mutants. (**A)** Outline of analyzed Elk-1 TAD mutants. Substrate sites were classified as fast (red), intermediate (blue) or slow (yellow) for model calculations. (**B**) Left: comparison of averaged measured data points of wild-type Elk-1 TAD fast-, intermediate- and slow-site phosphorylation by ERK2 (circles) with calculated rates according to the competitive inhibition model (solid lines). Center: fast-site alanine-substituted Elk-1 TAD (Elk-1F); dashed lines show wildtype Elk-1 TAD for comparison. Right: intermediate-site alanine-substituted Elk-1 TAD (Elk-1I); dashed lines show wildtype Elk-1 TAD for comparison. **(C)** Time-resolved

modification curves (right) of the Elk-1 369/423 switch mutant (left). Error bars denote differences between replicate experiments on two independent samples. **(D)** Time-resolved modification curves of ERK docking-site mutants Elk-1ΔD-box (left) and Elk-1ΔFQFP (right), presented as in (C). Effects of D-box and FQFP site deletions on Elk-1 TAD phosphorylation rates are summarised below.

Figure 3. Effects of Elk-1 TAD mutations on TCF target gene expression, cell proliferation and Mediator binding. **(A)** Quantitative reverse-transcription polymerase chain reaction (qRT-PCR) analysis of TCF target gene transcription in reconstituted TKO MEFs. Cells were reconstituted with wild-type mouse Elk-1 (WT) or fast-site (F), intermediate-site (I), slow-site (S), fast- and intermediate-site (FI) or alanine-substituted FW motif (FW) mutants. **(B)** Effects of individual slow-site alanine substitutions on *Egr1* expression. In (A) and (B) cells were stimulated with 50 ng/ml TPA where indicated. RNA levels are quantified relative to GAPDH; data are means ± SEM, n = 3. (**C**) Proliferation of wild-type and mutant Elk-1 TKO MEFs. Data are means ± SEM, n = 3. **(D)** Co-immunoprecipitation of Mediator with wildtype or mutant Flag-tagged Elk-1 from NIH3T3 cell extracts. Antibodies to Mediator subunits MED23, MED24 and MED16 were used for immunoblotting. **(E)** Mediator co-precipitation from unstimulated NIH3T3 cell extracts using wild-type and mutant GST-tagged Elk-1 TAD proteins with and without prior ERK2 phosphorylation.

Figure 4. Multisite phosphorylation of Elk-1 shapes the transcriptional response to ERK activation. **(A)** Kinetics of Elk-1 fast- and slow-site phosphorylation in cells treated with increasing concentrations of TPA. **(B)** Transcription rate of the TCF-SRF target gene *Egr1* in TKO MEFs expressing wildtype Elk-1 or mutant Elk-1S. Precursor RNA was monitored by qRT-PCR after stimulation with different concentrations of TPA. Data are mean ± SEM; n=3. **(C)** Kinetics of *Egr1* mRNA accumulation in cells as in (B) monitored by qRT-PCR **(D)** Progressive Elk-1 phosphorylation by ERK has both activating (left and center) and inhibitory (right) effects on Mediator recruitment, as suggested by shading densities. A strong signal will rapidly reach the attenuated state shown at the right, a weak signal may reach this state only if sustained.

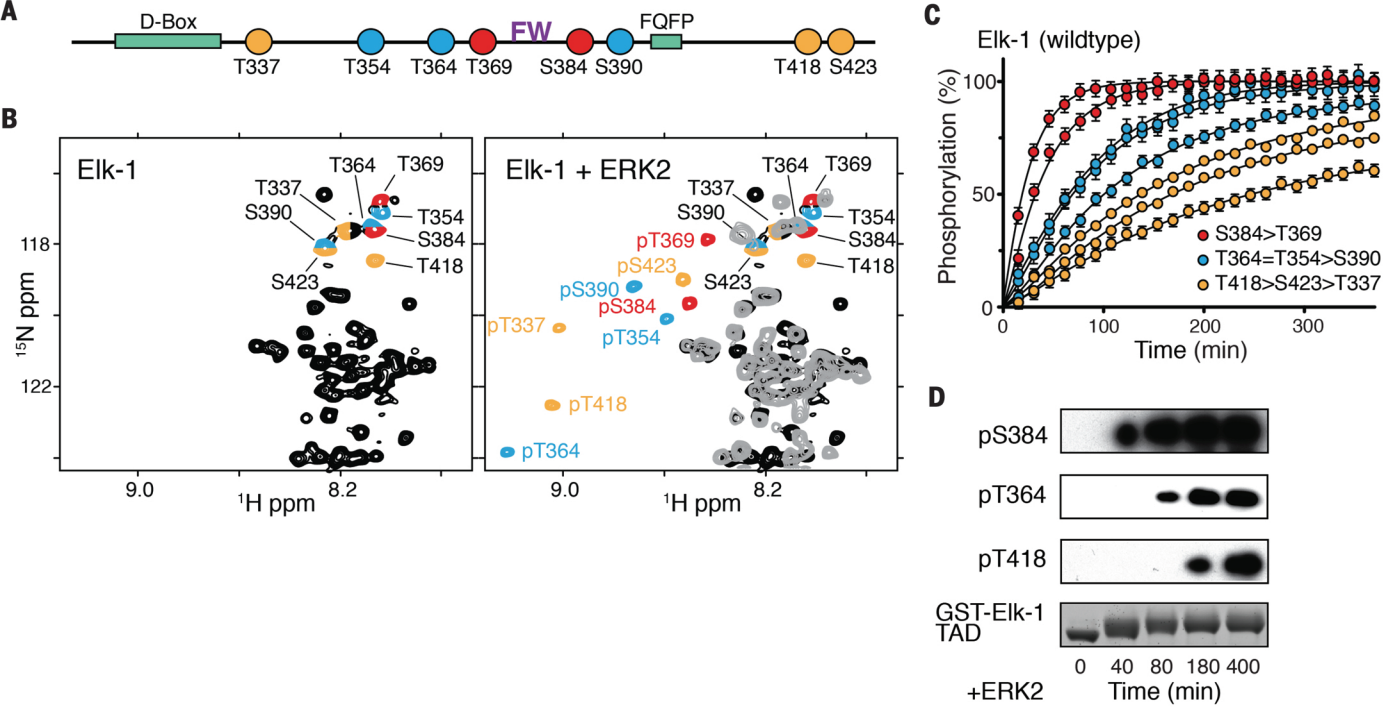
A
D-Box
FW
FQFP
T337
T354
T364
T369
S384
S390
T418
S423
B
Elk-1
Elk-1 + ERK2
^{15}N ppm
^{1}H ppm
118
122
9.0
8.2
pT369
pS423
pS390
pS384
pT337
pT354
pT418
pT364
C
Elk-1 (wildtype)
Phosphorylation (%)
100
50
0
100
200
300
Time (min)
S384>T369
T364=T354>S390
T418>S423>T337
D
pS384
pT364
pT418
GST-Elk-1 TAD
0 40 80 180 400
+ERK2
Time (min)

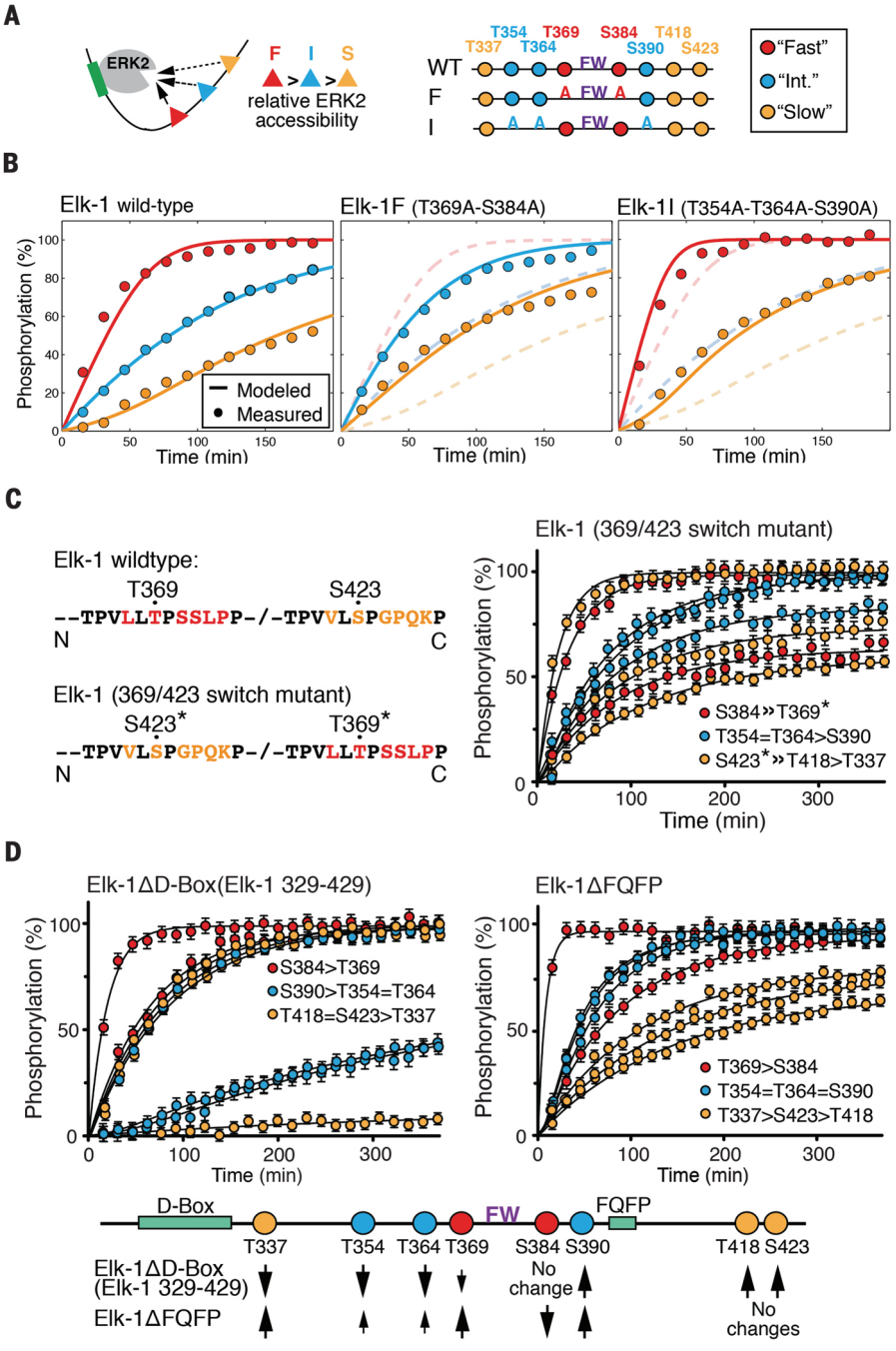
A
ERK2
F I S
relative ERK2 accessibility
T354 T369 S384 T418
T337 T364 S390 S423
WT FW
F A FW A
I A A FW A
"Fast"
"Int."
"Slow"
B
Elk-1 wild-type
Elk-1F (T369A-S384A)
Elk-1I (T354A-T364A-S390A)
Phosphorylation (%)
Modeled
Measured
Time (min)
C
Elk-1 wildtype:
T369 S423
--TPVLLTPSSLPP-/-TPVVLSPGPQKP
N C
Elk-1 (369/423 switch mutant)
S423* T369*
--TPVVLSPGPQKP-/-TPVLLTPSSLPP
N C
Elk-1 (369/423 switch mutant)
S384»T369*
T354=T364>S390
S423*»T418>T337
D
Elk-1ΔD-Box(Elk-1 329-429)
S384>T369
S390>T354=T364
T418=S423>T337
Elk-1ΔFQFP
T369>S384
T354=T364=S390
T337>S423>T418
D-Box
FW
FQFP
T337 T354 T364 T369 S384 S390 T418 S423
Elk-1ΔD-Box (Elk-1 329-429)
Elk-1ΔFQFP
No change
No changes

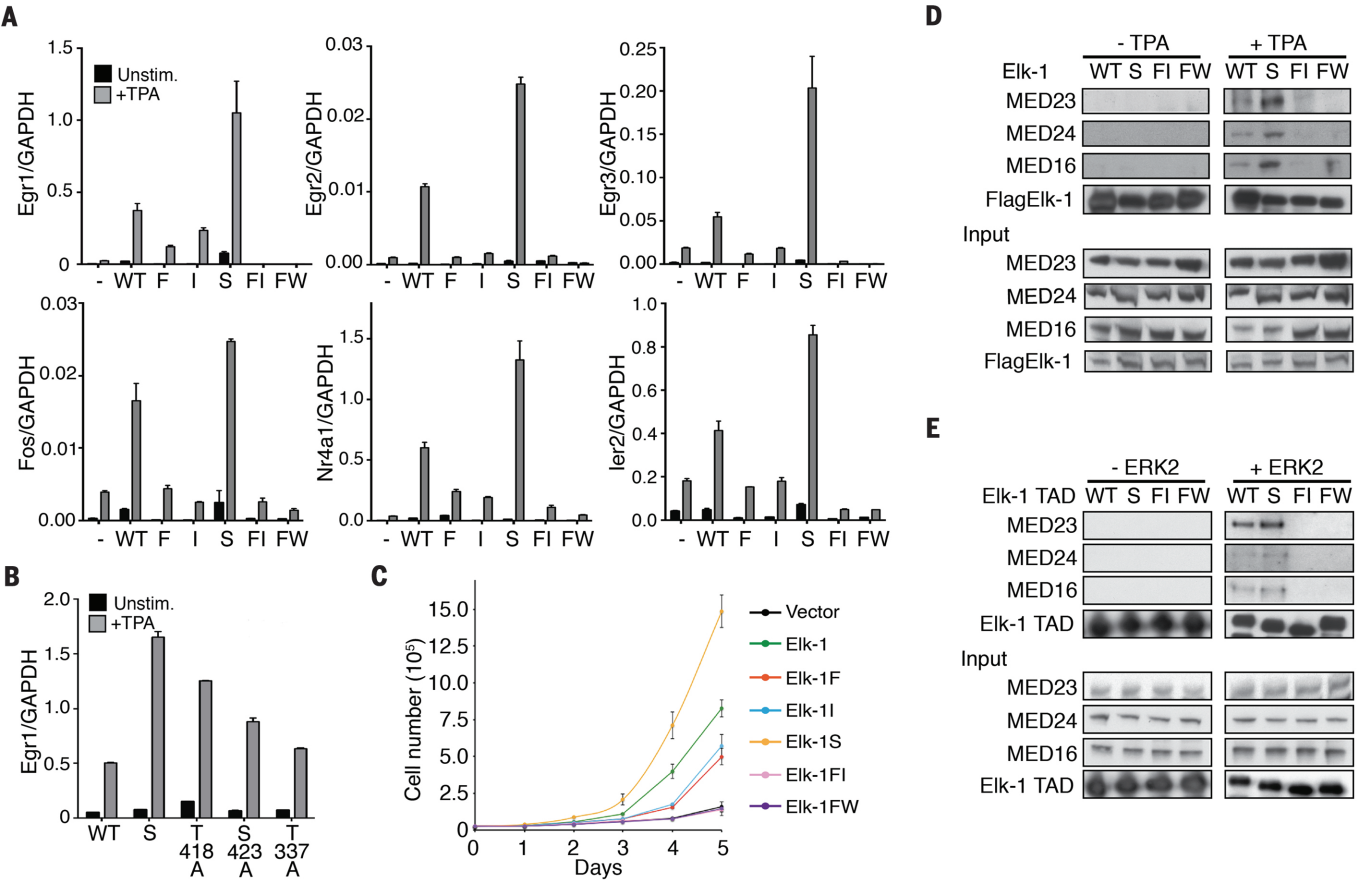
A
Unstim.
+TPA
Egr1/GAPDH
Egr2/GAPDH
Egr3/GAPDH
Fos/GAPDH
Nr4a1/GAPDH
Ier2/GAPDH
- WT F I S FI FW
B
Unstim.
+TPA
Egr1/GAPDH
WT
S
T 418 A
S 423 A
T 337 A
C
Cell number (10^5)
Days
Vector
Elk-1
Elk-1F
Elk-1I
Elk-1S
Elk-1FI
Elk-1FW
D
- TPA
+ TPA
Elk-1
WT S FI FW
MED23
MED24
MED16
FlagElk-1
Input
E
- ERK2
+ ERK2
Elk-1 TAD

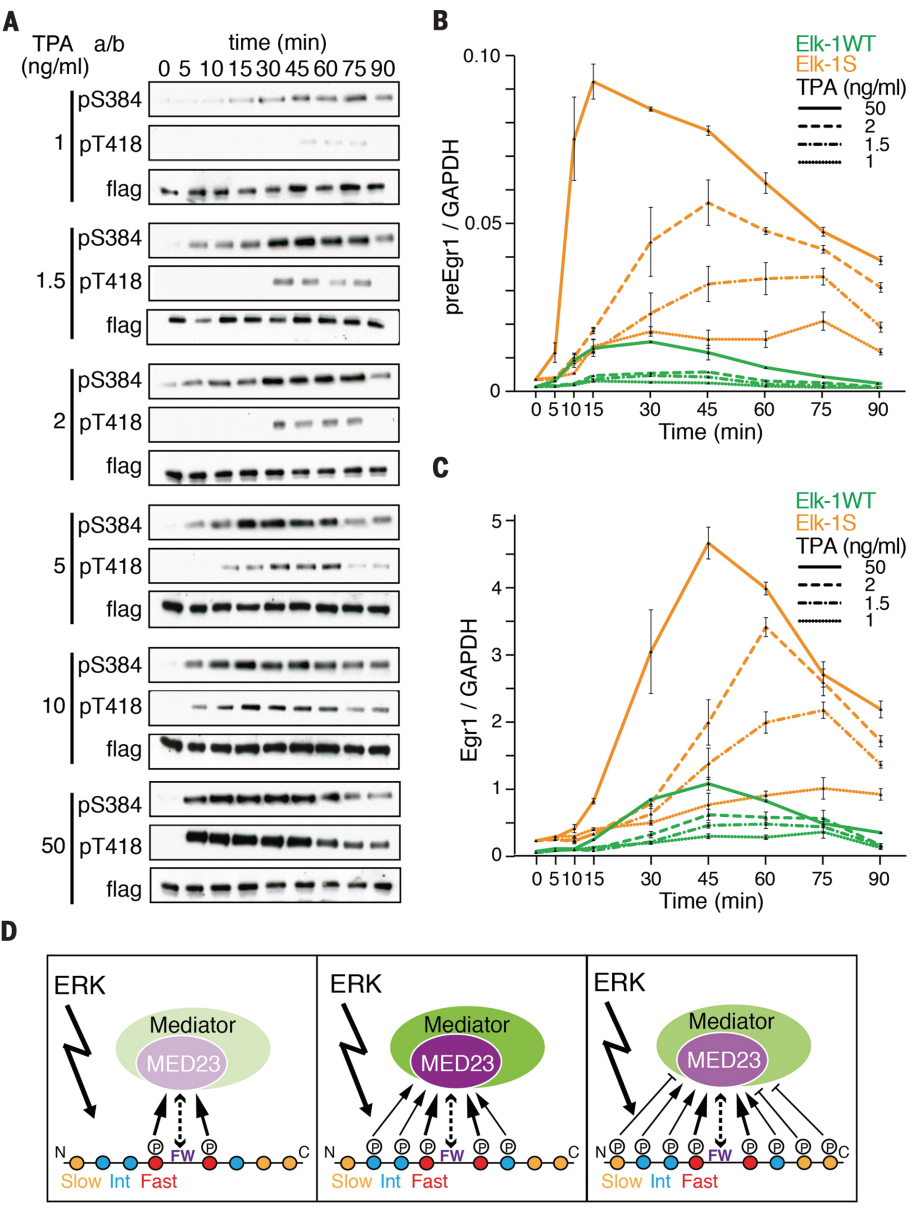
A
TPA (ng/ml)
a/b
time (min)
0 5 10 15 30 45 60 75 90
1
1.5
2
5
10
50
pS384
pT418
flag
B
Elk-1WT
Elk-1S
TPA (ng/ml)
50
2
1.5
1
preEgr1 / GAPDH
0.10
0.05
0
0 5 10 15 30 45 60 75 90
Time (min)
C
Elk-1WT
Elk-1S
TPA (ng/ml)
50
2
1.5
1
Egr1 / GAPDH
5
4
3
2
1
0
0 5 10 15 30 45 60 75 90
Time (min)
D
ERK
Mediator
MED23
N
C
P
FW
Slow Int Fast

Materials and Methods

Molecular techniques

Plasmid constructions, protein analysis by SDS-PAGE and immunoblotting, siRNA-mediated protein depletion, and cell proliferation analysis used standard methods.

Recombinant GST-Elk-1 TAD.

Wild-type or mutant mouse Elk-1 sequences encoding residues 309-429 were expressed as GST-$(His)_6$ fusion proteins, inserted between BamHI and NotI sites of modified pET-41a (*30*). Protein expression was induced in *E. coli* BL21(DE3) (Novagen) with 0.5 mM IPTG at 37° C. Cells were lysed in 50 mM Tris pH 8.0, 300 mM NaCl, 5 mM DTT, with Complete protease inhibitor cocktail (Roche Diagnostics). Cleared lysates were applied to glutathione Sepharose resin (GE Healthcare Life Sciences) and washed extensively with lysis buffer. Proteins were eluted with 20mM reduced glutathione in 50 mM Tris pH 8.0, 150 mM NaCl, 5mM DTT, and further purified on a Superdex 200 HR10/30 size exclusion column (GE Healthcare Life Sciences) in 20 mM K_2HPO_4 pH 6.8, 150 mM NaCl, 5 mM DTT. For ^{15}N- and ^{15}N-/^{13}C-labeling, growing cells were transferred to minimal medium containing $^{15}NH_4Cl$ and/or ^{13}C-glucose as appropriate and grown at 30 °C. After adsorption to glutathione sepharose the Elk-1 moiety was released by incubation with 1:50 (w/w) GST-3C protease on the resin, and purified by Superdex 75 HR10/30 size exclusion chromatography as above. For phosphorylation, GST-Elk-1 TAD proteins (50μM) were incubated with 400 U ERK2 (NEB) in 100μl 10 mM K_2HPO_4 pH 6.9, 50 mM NaCl, 1 mM ATP, 2mM DTT, 5 mM $MgCl_2$ at 25 °C.

NMR spectroscopy

All NMR experiments were performed on a 750 MHz Bruker NMR spectrometer equipped with cryogenically cooled triple resonance probe (TCI). Resonance assignments for WT and mutant Elk-1 TAD were obtained by 2D ^1H-^{15}N HSQC and 3D HNCACB, HN(CA)CO, CA(CO)NNH, HNCO, (H)N(CA)NH NMR experiments with uniformly ^{15}N- and ^{13}C-labeled samples in 10 mM Na_3PO_4, 50 mM NaCl, pH 6.4, 10% D_2O, at 25 °C. 3D HNCACB experiments were recorded with 512 (t_3) × 64 (t_2) × 42 (t_1) complex data points for ^1H, ^{13}C and ^{15}N dimensions, respectively, HN(CA)CO experiments with 512 (t_3) × 32 (t_2) × 40 (t_1) complex points, CA(CO)NNH experiments with 512 (t_3) × 44 (t_2) × 36 (t_1) complex points, HNCO experiments with 512 (t_3) × 48 (t_2) × 64 (t_1) complex points, (H)N(CA)NH experiments with 512 (t_3) × 44 (t_2) × 44 (t_1) complex points. 2D HSQC experiments were recorded with 512 (t_2) × 128 (t_1) complex points. All 3D NMR spectra were processed with Topspin 3.1 and analyzed in CcpNMR. Final ^1H and ^{15}N amide assignments at pH 6.8 and 298 K were obtained by following progressive cross-peak displacements from pH 6.4 and 277 K to pH 6.4 and 298 K (5 steps: 277 K, 283 K, 288 K, 293 K, 298 K), and from pH 6.4 and 298 K to pH 6.8 and 298 K. Assignments of unmodified and phosphorylated wild-type Elk-1 TAD, as well as details of NMR experiments used to derive them have been deposited in the Biological Magnetic Resonance Data Bank (BMRB, accession numbers 26762 and 26786, respectively).

For time-resolved NMR monitoring of Elk-1 phosphorylation reactions, samples were reconstituted with ^{15}N isotope-labeled Elk-1 TAD (50 μM in 100 μl sample volume 10 mM Na_3PO_4, 50 mM NaCl, 1 mM ATP, 2 mM DTT, 5 mM $MgCl_2$, 10% D_2O, pH 6.9)

and 400 U ERK2 (NEB), or 200 U p38α (Signal Chem), 375 U JNK1, or 375 U JNK2 (both Proqinase) at 25 °C. Progressive phosphorylation was analyzed and quantified as described previously (*20*). Error bars represent the precision with which individual phosphorylation levels were determined for each time point. They reflect the number of uniquely resolved chemical shifts whose peak intensities reported on the modification states of respective ERK2 sites (i.e. phosphorylated serines and threonines, and flanking residues). Intensities of at least two independent NMR signals reporting on the same phosphorylation event were combined for each time point (determined relative to normalized intensities of fully modified sites). Larger error bars represent sites for which fewer signals were combined (= 2), smaller error bars correspond to sites for which greater numbers of peak intensities were integrated (> 2). For measurement points without error bars, the determined experimental precision is smaller than the chosen point size. All time-resolved NMR measurements of individual phosphorylation reactions were repeated on at least two independent replicate samples (n=2) under identical experimental conditions and with the same kinase batch. Error bars reflecting the reproducibility of such measurements are smaller than the chosen point size (ie the circles in the figures; not shown).

Consecutive 2D ^{1}H-^{15}N SOFAST-HQMC experiments were recorded with 64 scans, 40 ms interscan delays, and 512 (t_2) × 64 (t_1) complex points. Individual acquisition times were 15 min and 30 s. All NMR spectra were processed by linear prediction in the ^{15}N dimension (64 complex points), cosine-bell apodization and zero filling to 4,096 (t_2) and 2,048 (t_1) data points, processed with Topspin 3.1 and analyzed in Sparky. Assignment of NMR signals of phosphorylated WT and mutant Elk-1 TAD was based on additional sets of 3D HNCACB experiments and de-novo backbone assignment procedures. Combined ^{1}H and ^{15}N, ^{13}CO chemical shift differences (Δδ) between unmodified and phosphorylated Elk-1 TAD were calculated as $\Delta\delta = [(\Delta\delta_{HN}^2 + (\Delta\delta_{N}*0.154)^2 + (\Delta\delta_{CO}*0.351)^2)^{1/2}]/3$ and plotted for each residue, except prolines (*31*). Secondary structure propensities of unmodified and phosphorylated Elk-1 TAD were obtained with the neighbor-corrected structural propensity calculator (*32, 33*) (http://nmr.chem.rug.nl/cgi-bin/selection_screen_ncSPC.py) using experimentally determined Cα and Cβ chemical shifts as input. Random coil chemical shift values of glycines preceding prolines were corrected to –0.77 p.p.m. according to (*34*). Similarly, random coil chemical shift values of phosphorylated serines and threonines were corrected as outlined in (*35*), also by taking pH-dependent chemical shift changes into account (*36*). Hence, the following correction values were used for chemical shift measurements at pH 6.9: For pSer, $\delta(C\alpha)_{corr} = \delta(C\alpha)+0.012$ and $\delta(C\beta)_{corr} = \delta(C\beta)-1.865$, for pThr, $\delta(C\alpha)_{corr} = \delta(C\alpha)-1.16$ and $\delta(C\beta)_{corr} = \delta(C\beta)-2.33$ (in p.p.m.).

Multisite phosphorylation model

The rate of Elk-1 phosphorylation *in vitro* is dependent on the concentration of ERK2 (fig. S3A), suggesting an apparently distributive phosphorylation mechanism where ERK2 modifies one phosphorylation site per docking encounter with Elk-1 (*37*). Since Elk-1 is released from ERK2 after each phosphorylation step, at each substrate encounter the different phosphorylation sites will effectively compete for ERK2. To simplify the mathematical treatment, we arbitrarily grouped the slower phosphorylation sites according to their distance from the midpoint between the two fastest sites (Fast,

T369 and S384; Intermediate: T354, T364, S389; Slow, T337, T418, S423), with decreasing relative affinities for ERK2 (ie $K_M^{Fast} < K_M^{Int} < K_M^{Slow}$). The phosphorylation kinetics for wild-type Elk-1, with the Fast, Intermediate, and Slow sites were fitted according to equations 1 and 2 (*20, 38*). These equations describe the kinetics for a pair of sites competing for ERK2. As illustrated, equations (1) and (2) represent the relation between the Fast and Slow sites; similar equations can be applied to describe the other pairwise relationships between the different site classes. The δ value, defined in equation 2, indicates the degree of competition between the sites (δ=1 denotes equal competition between sites, while 0<δ<<1 denotes weak competition).

$$\frac{[pS_{fast}](t)}{[S]_{(t=0)}} = 1 - \left(\frac{1 + \frac{[S]_{(t=0)}}{K_M^{slow}}}{\frac{[S]_{(t=0)}}{K_M^{fast}}} * \ln\left(1 + \left[\exp\left(\frac{\frac{[S]_{(t=0)}}{K_M^{fast}}}{1 + \frac{[S]_{(t=0)}}{K_M^{slow}}} \right) - 1 \right] * \exp\left(- \frac{\frac{V_{max}^{fast}}{K_M^{fast}} * t}{1 + \frac{[S]_{(t=0)}}{K_M^{slow}}} \right) \right) \right) \qquad (1)$$

$$\frac{[pS_{slow}](t)}{[S]_{(t=0)}} = 1 - \left(1 - \frac{[pS_{fast}](t)}{[S]_{(t=0)}} \right)^{\delta} \qquad (2)$$

$$\delta = \frac{V_{max}^{slow} \times K_M^{fast}}{K_M^{slow} \times V_{max}^{fast}}$$

Where:
[S] is concentration of the phosphorylation sites; K_M^{Fast}, K_M^{Int} and K_M^{Slow} are the apparent Michaelis-Menten constants for the Fast, Intermediate and Slow groups of sites respectively; V_{max}^{Fast}, V_{max}^{Int} and V_{max}^{Slow} are maximum rates of phosphorylation for the Fast, Intermediate and Slow groups of sites respectively (proportional to the modification turnover rates); δ is the competitive index. Note that Equation 2 is a corrected form (*20, 39*). Complete derivation of these kinetic formulas is published elsewhere (*20, 38*).

The observed data for the wild-type protein were fitted to the competition model in Fig. 2B, left panel, which defined the parameters that determine the δ values as: $\frac{[S]_{(t=0)}}{K_M^{fast}}$ = 12.7, $\frac{[S]_{(t=0)}}{K_M^{int}}$ = 3.34, $\frac{[S]_{(t=0)}}{K_M^{slow}}$ = 2.65, $\frac{V_{max}^{fast}}{K_M^{fast}}$=0.14 min^{-1}, $\frac{V_{max}^{int}}{K_M^{int}}$ = 0.029 min^{-1}, and δ values as: Fast vs Slow, δ = 0.10; Fast vs Int, δ = 0.26; Int vs Slow, δ = 0.43.

The data for the different Elk-1 mutants were then modeled assuming that the competitive relationships between the different types of sites are maintained in the mutants, and that mutated sites have negligible affinity for the kinase. The Elk-1F mutant data fit the model well, with the kinetics of intermediate and slow site phosphorylation in the mutant approaching those of the wild-type fast and intermediate sites respectively (Fig. 2B, center). The Elk-1I mutant data also fitted the model well, with the kinetics of

the fast sites increasing relative to wild-type, and the rate of slow site phosphorylation approaching that of the intermediate sites in wild-type Elk-1 (Fig. 2B, right).

Expression and analysis of wild-type and mutant mouse Elk-1 in triply TCF-deficient MEFs

Triply TCF-deficient (TKO) MEFs, lacking Elk-1, Net, and SAP-1, were prepared from $Elk1^{-/-}$;$Elk3^{\delta/\delta}$;$Elk4^{-/-}$ embryos (*40*) and immortalized using SV40 T antigen (gift from Victoria Lawson). DNA encoding N-terminally flag-tagged full-length wild-type and mutant mouse Elk-1 were synthesized (GeneArt-Life technologies) and expressed using pMIG/MSCV-IRES-GFP (*41*). Cell sorting by GFP was used to isolate populations with similar levels of Elk-1 expression and confirmed by immunoblotting. Elk-1 mutants were: Elk-1F, T369A, S384A; Elk-1I, T354A, T364A, S390A; Elk-1S, T337A, T418A, S423A; Elk-1FI, T354A, T364A, T369A, S384A, S390A; Elk-1FW, F379A, W380A, Elk-1 T418A; Elk-1 S423A; Elk-1 T337A.

For functional analysis, TKO cells expressing wild-type and mutant Elk-1 were grown in triplicate cultures in 6-well plates, serum-starved for 48 h, then stimulated with TPA. For gene expression analysis, RNA was prepared at the time of peak mRNA accumulation (*Egr1*, 45'; *Egr2*, 90'; *Egr3*, 120'; *Fos*, 45'; *Nr4a1*, 60'; *Ier2*, 45'), or over a time course, using the GenElute 96 well Total RNA purification kit (Sigma-Aldrich). cDNA was synthesized using the Transcriptor First Strand cDNA Synthesis Kit (Roche), and quantitative PCR was performed using an ABI 7900 thermocycler (Applied Biosystems) sequence detection system with SYBR green incorporation (Invitrogen, Carlsbad, CA). Relative abundance of template cDNA was calculated by the ΔCt method, normalizing to the abundance of Glyceradelhyde 3-phosphate dehydrogenase (GAPDH) cDNA. Primers for mRNA qPCR analysis were as described previously (*40*). *Egr1* intronic primers were TGATGTCTCCGCTGCAGATC and GGTGGGTGAGTGAGGAAAGG. For phosphorylation at 25 °C, cells were equilibrated at 25 °C for 1h before stimulation. Lysates for SDS-PAGE were prepared in 150 µl 2x SDS sample buffer and treated with Benzonase for 30 min, at 37 °C. Growth rates of TKO cells expressing wild-type and mutant Elk-1 were assessed by plating 2.5×10^4 cells in triplicate for each cell lines, with trypsinization and counting each day over 5 days. For siRNA depletion experiments, cells were transfected with 20 nmol siRNA oligonucleotides using Lipofectamine RNAi MAX (Invitrogen) Control siRNA was All Star (Qiagen). SMARTPOOL mouse MED23 siRNA was from Dharmacon.

Immunoprecipitation, GST-fusion affinity assays, and antibodies

Cells were lysed in PBS, 0.1% NP-40, 1 mM Na_3VO_4, 1mM okadaic acid and protease inhibitor cocktail (Roche Diagnostics), sonicated, and cleared by centrifugation for 15 min at 13000 rpm at 4 °C. For co-immunoprecipitation, lysates were incubated with 20 µl anti-flag M2 magnetic beads for 3 h at 4 °C. For GST-fusion protein affinity assays, 20 µl of gluthatione sepharose beads containing ~10 µg GST fusion protein, with binding for 3 h at 4 °C. Beads were washed 3 times with lysis buffer, and proteins were eluted with 20 µl of 1x SDS loading buffer. Standard transient transfection procedures were used to express HA-MED23 in NIH3T3 cells. Immunoprecipitation and GST fusion protein affinity assays were performed at least three times. Antibodies were: Flag (rabbit), flag M2 peroxidase (HRP), GST (rabbit), Sigma-Aldrich; GFP (rabbit), MCM6

(goat), Santa Cruz Biotechnology; MED23 (mouse), BD Biosciences; MED16 (rabbit), MED24 (rabbit), Bethyl Laboratories; ERK (panERK) (mouse), BD Transduction Laboratories; P-p44/42 MAPK (pERK) (rabbit), phospho-Elk-1(Ser383) (mouse), Cell Signaling; phospho-Elk-1(Thr363) (rabbit) phospho-Elk-1(Thr417) rabbit, in-house (*6*).

Fig. S1.

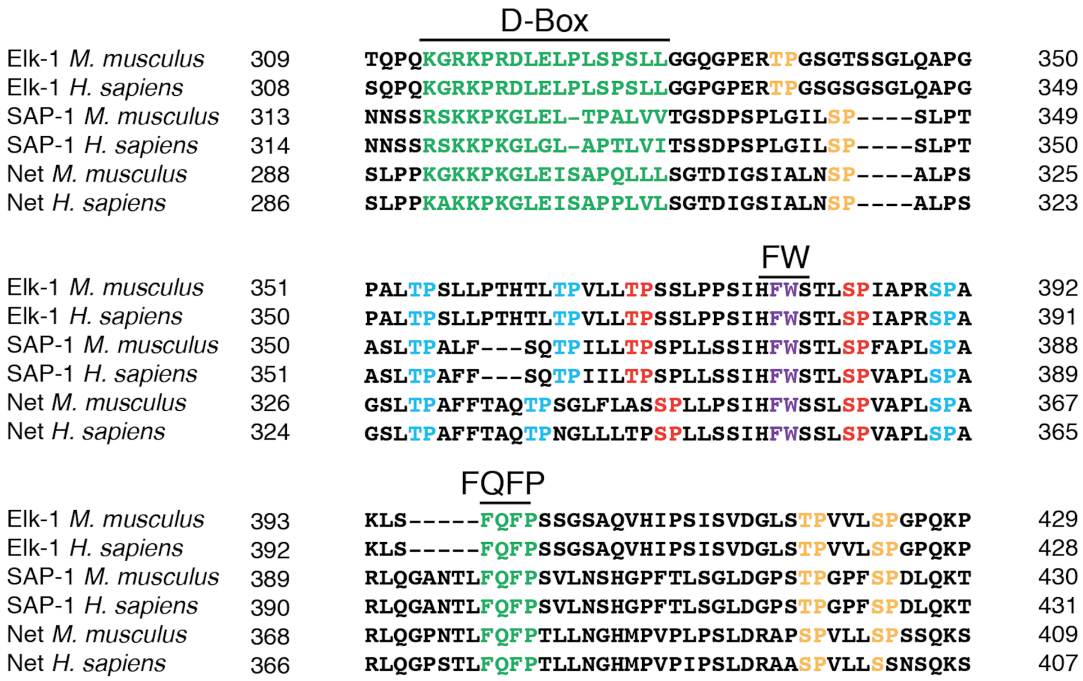

Sequence conservation of human and mouse Elk-1, SAP-1 and Net TADs. Conserved S/T-P phosphorylation sites are highlighted according to Elk-1/ERK2 modification rates as fast, red; intermediate, blue; and slow, yellow. The D-box and FQFP kinase docking motifs are shown in green and the central FW Mediator-binding motif in purple.

Fig. S2

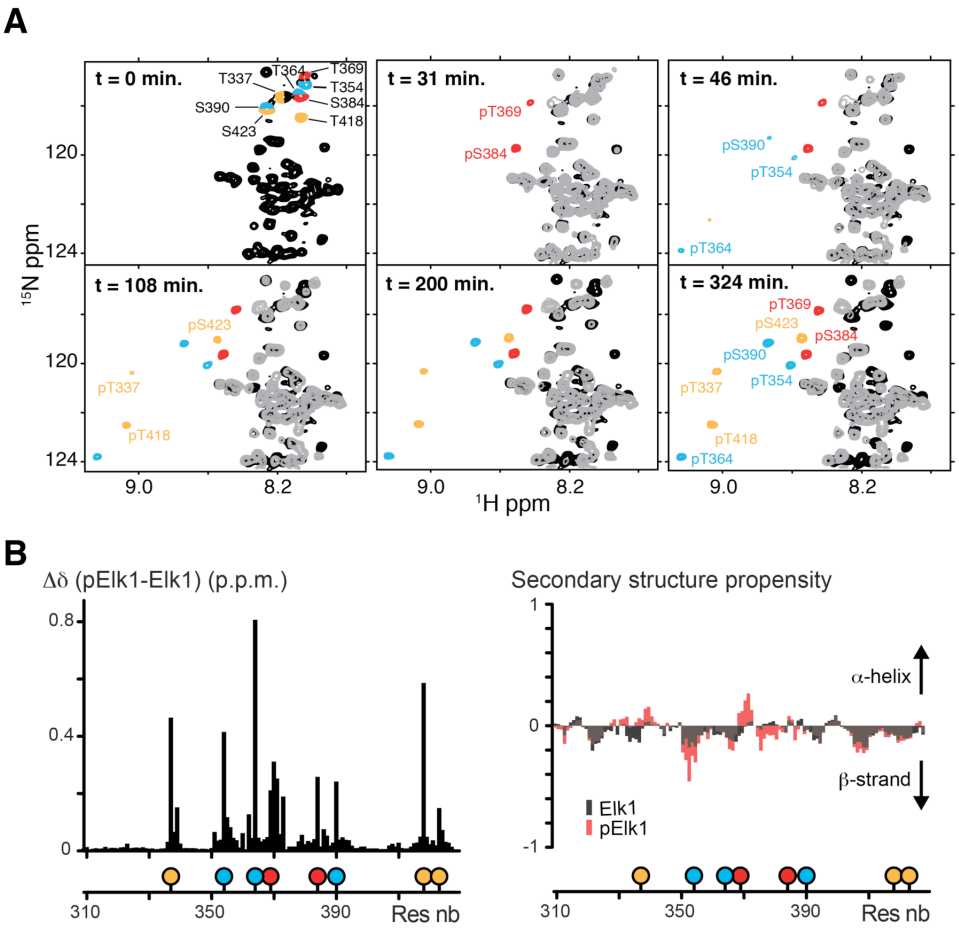

NMR analysis of Elk-1 TAD phosphorylation by ERK2. (**A**) Time-resolved 2D NMR spectra of reconstituted phosphorylation reactions with ^{15}N-labeled Elk-1 TAD (aa309-429) and recombinant, unlabeled ERK2 at indicated reaction time-points. Phospho-site serine-threonine residues are color-coded according to their modification rates, i.e., fast (red), intermediate (blue) and slow (yellow). Progressive appearance of down-field shifted resonance cross-peaks, corresponding to phosphorylated serine-threonine residues, illustrates the time-dependent phosphorylation behavior of individual Elk-1 TAD sites. Grey cross-peaks denote all other Elk-1 TAD residues. (**B**) Left, chemical shift difference (δΔ) analysis between unmodified and phosphorylated Elk-1 TAD with δΔ values plotted for each residue, except prolines, according to (*31*). As expected, Δδ values are highest for phosphorylated Elk-1 TAD residues, with minor changes for neighboring residues, and readily identify modified substrate sites. Right, residue-resolved secondary structure propensity calculations for unmodified (black) and phosphorylated (red) Elk-1 TAD (*32, 33*)using experimentally determined Cα and Cβ chemical shift values as input. As can be appreciated from this plot, overall residual secondary structure propensities are below ~20 % in both forms of Elk-1 TAD and not substantially altered upon multisite phosphorylation. Hence, unmodified and phosphorylated Elk-1 TADs populate structural states that are largely disordered.

Fig. S3

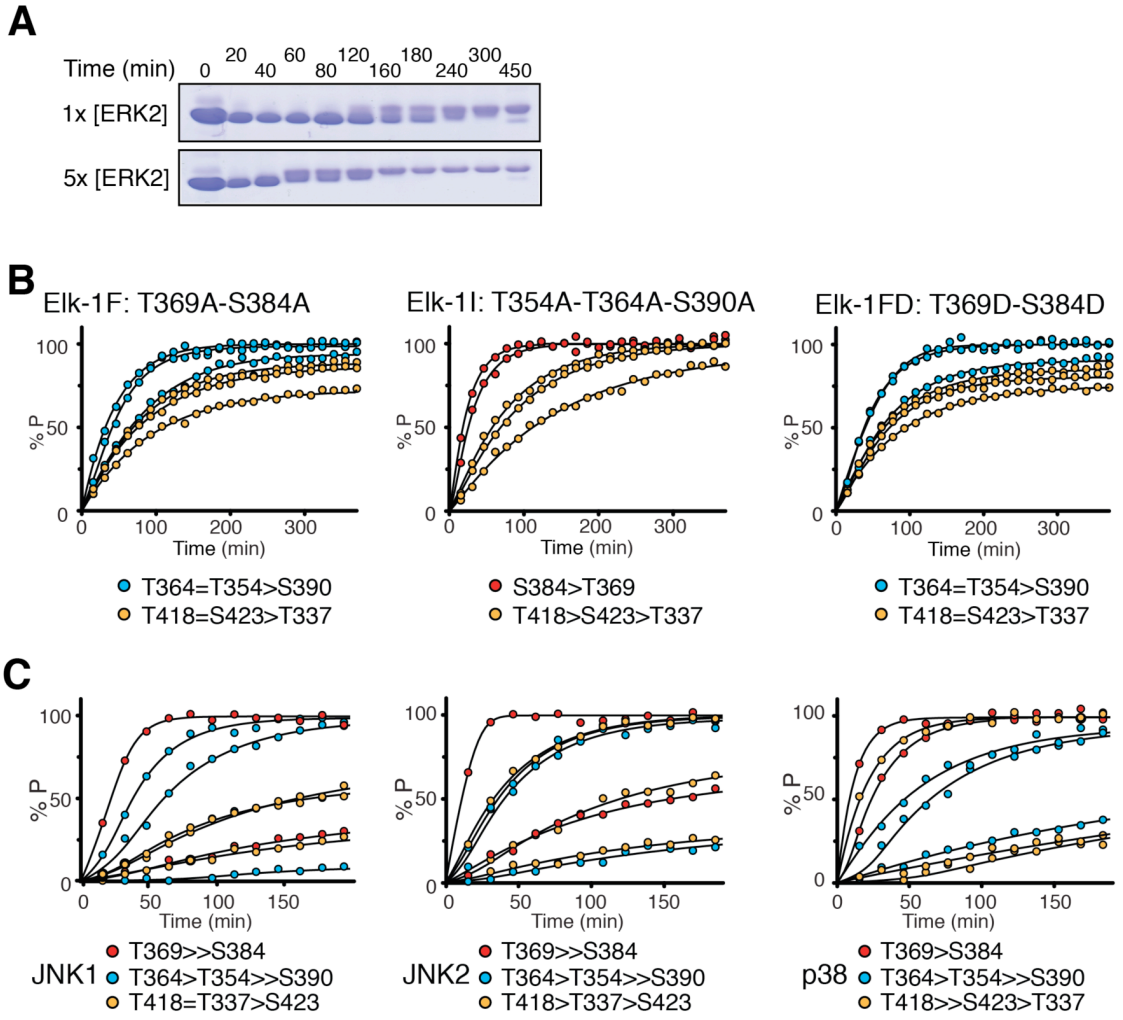

Time-resolved phosphorylation behavior of wild-type and mutant Elk1-TAD (**A**) SDS-PAGE analysis of phosphorylation kinetics of GST-Elk-1 TAD using low and high amounts of ERK2. (**B**) Representative time-resolved modification curves of individual Elk-1 TAD sites upon phosphorylation with ERK2 using fast- (Elk-1F, T369A-S384A) and intermediate-site mutants (Elk-1I, T354A-T364A-S390A) as substrates, as well as fast-site aspartate-substituted Elk-1 TAD (Elk-1FD, T369D-S384D). (**C**) Representative time-resolved modification curves of individual Elk-1 sites upon phosphorylation with JNK1, JNK2 and p38 MAP kinases. Sites are color-coded according to their ERK2 rates. Elk-1 TAD phosphorylation by JNK exhibited a strong kinetic preference for T-P motifs, reminiscent of ERK2 phosphorylation of the FQFP mutant, and consistent with observations showing that JNK does not interact with the FQFP docking site (*14, 15*). TAD phosphorylation by p38 was more similar to ERK2 consistent with p38's ability to interact with FQFP (*25*).

Fig. S4

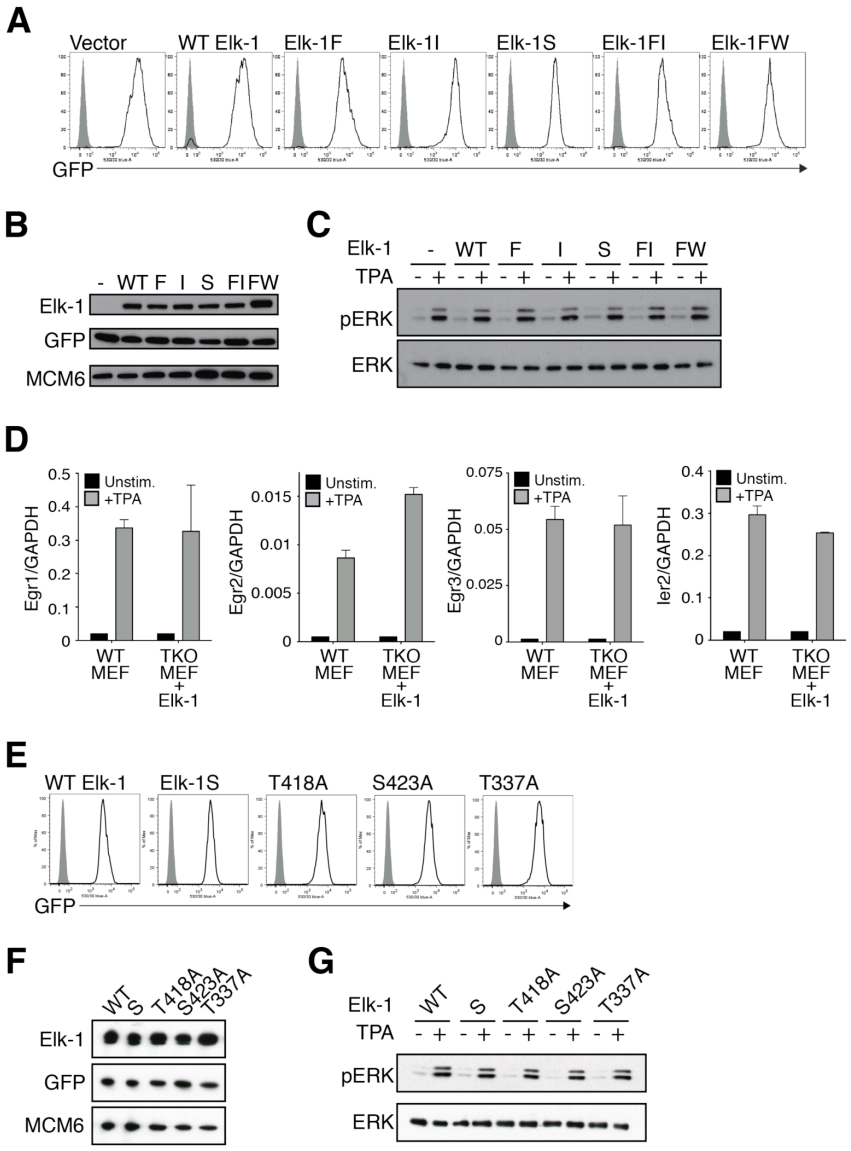

Reconstitution of TCF-deficient MEFs (TKO MEFs) with wild-type or mutant mouse Elk-1. (**A**) Reconstituted TKO cells expressing wild-type Elk-1, Elk-1F, Elk-1I, Elk-1S, Elk-1FI, or Elk-1FW at comparable levels, as confirmed by FACS analysis of the co-expressed GFP marker and (**B**) immunoblotting with anti-Flag antibody. **(C)** ERK activation upon TPA stimulation was comparable in all lines. (**D**) Comparison of TCF-SRF target gene expression in wild-type MEFs and TCF-deficient MEFs (TKO MEFs) reconstituted with wild-type Elk-1. Cells were stimulated with TPA and transcripts quantified by qRT-PCR (relative to GAPDH RNA). Data are mean ± SEM (n=3). (**E-G**) Reconstituted TKO cells expressing wild-type Elk-1, Elk-1S, Elk-1T418A, Elk-1S423A and Elk-1T337A. (**E**) Elk-1 protein levels were comparable, as confirmed by FACS analysis of the co-expressed GFP marker, and (**F**) immunoblotting with anti-Flag antibody (**G**) ERK activation upon TPA stimulation was comparable in all lines.

Fig. S5

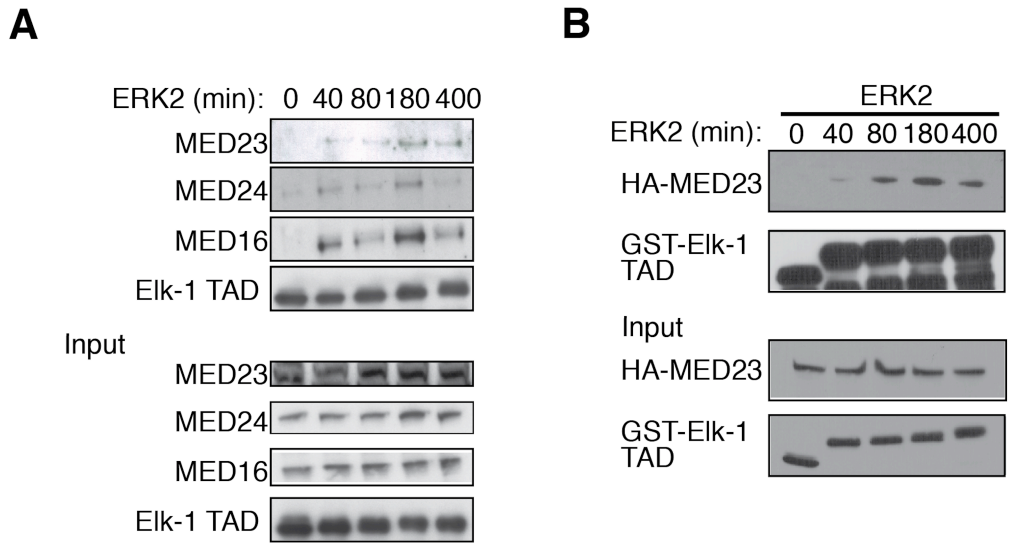

Effect of Elk-1 phosphorylation on Mediator interaction. (**A**) Mediator co-precipitation from unstimulated NIH3T3 cell extracts using wild-type GST-tagged Elk-1 TAD proteins phosphorylated for the indicated times with ERK2, detected by immunoblotting for MED23, MED16 and MED24. (**B**) Affinity precipitation as in (A) but from extracts of NIH3T3 cells transiently expressing HA-MED23.

Fig. S6

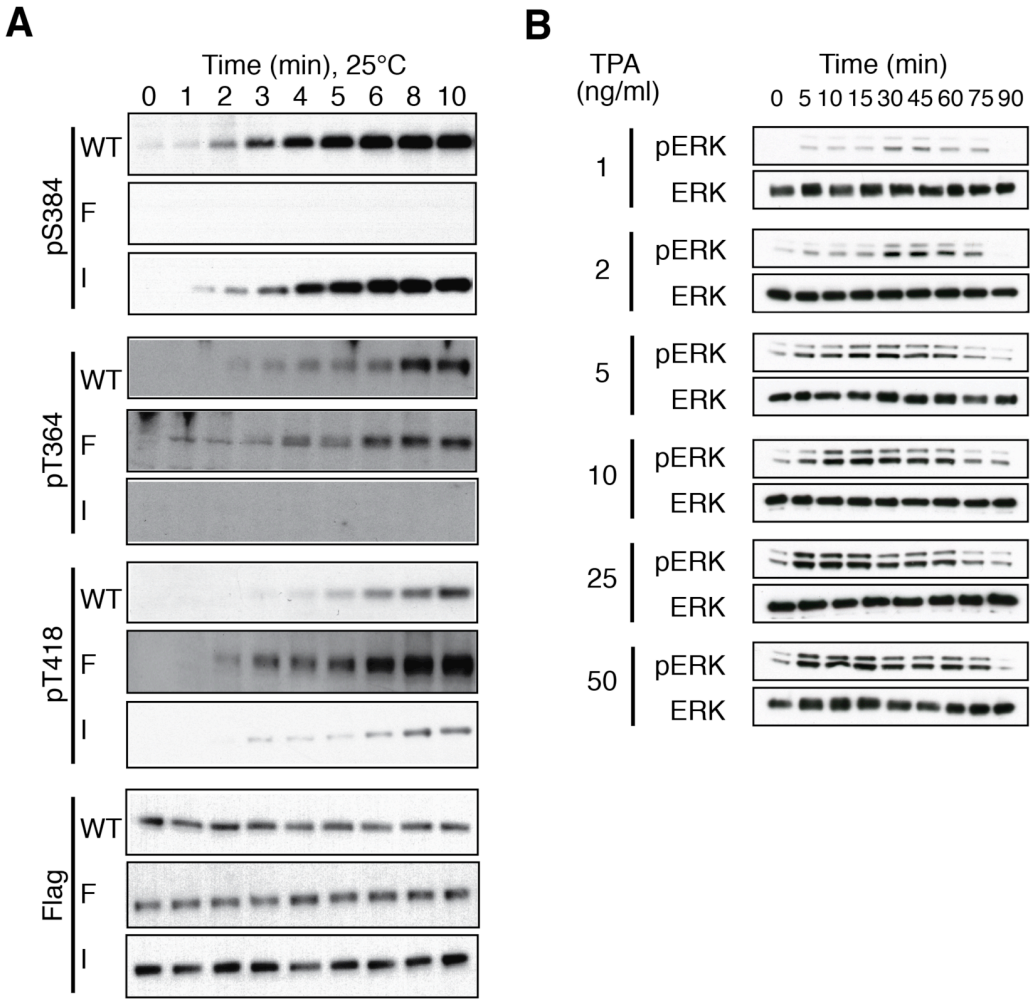

Time course of Elk-1 phosphorylation and ERK activation upon differential TPA stimulation (**A**) Phosphorylation of fast (pS384), intermediate (pT364) and slow (pT418) Elk-1 sites in TCF-deficient MEFs reconstituted with mouse Elk-1 mutants upon stimulation with 50 ng/ml TPA at 25° C. (**B**) Immunoblot analysis of ERK phosphorylation/activation in MEFs reconstituted with wild-type Elk-1 and stimulated with increasing amounts of TPA at 37° C.